Strain-Dependent Solid Surface Stress and the Stiffness of Soft Contacts

Katharine E. Jensen,[*] Robert W. Style, Qin Xu, and Eric R. Dufresne[†]

Department of Materials, ETH Zürich, Switzerland

(Received 10 July 2017; revised manuscript received 7 September 2017; published 9 November 2017)

Surface stresses have recently emerged as a key player in the mechanics of highly compliant solids. The classic theories of contact mechanics describe adhesion with a compliant substrate as a competition between surface energies driving deformation to establish contact and bulk elasticity resisting this. However, it has recently been shown that surface stresses provide an additional restoring force that can compete with and even dominate over elasticity in highly compliant materials, especially when length scales are small compared to the ratio of the surface stress to the elastic modulus, Υ/E. Here, we investigate experimentally the contribution of surface stresses to the total force of adhesion. We find that the elastic and capillary contributions to the adhesive force are of similar magnitude and that both are required to account for measured adhesive forces between rigid silica spheres and compliant, silicone gels. Notably, the strain dependence of the solid surface stress contributes to the stiffness of soft solid contacts at leading order.

Soft solids can make excellent adhesives because they can conform to establish intimate contact, even on very rough surfaces [1,2]. Applications of soft or "pressure-sensitive" adhesives range from the ubiquitous sticky note to large-scale building construction [2], from everyday adhesive bandages to new developments toward improved surgical techniques [3]. The true test of any adhesive material is how it responds to an externally applied force. Does it stick and stay stuck, and how much force can it sustain before unsticking? Even though soft adhesives are widely used, answering these seemingly simple questions remains an area of active research [4–14].

When a soft solid conforms into adhesive contact with an uneven surface, it is well understood that bulk elasticity opposes this deformation [15–17]. However, a number of recent experiments have demonstrated that for highly compliant solids, elasticity is not always enough to describe the mechanical response [6,18–31]. Rather, an additional restoring force can arise from the solid surface tension Υ, which opposes the stretching of the surface required to conform into contact. This solid surface stress can compete with or even dominate over the elastic modulus E in determining the mechanics of soft materials, at least on length scales that are small compared to an elastocapillary length, $L_c = \Upsilon/E$.

[*]Present address: Williams College Department of Physics, Williamstown, MA, USA;
kej2@williams.edu
[†]eric.dufresne@mat.ethz.ch

Meanwhile, surface stresses are still ignored in the standard theories of adhesive contact mechanics [15–17]. Recent insights into elastocapillary phenomena suggest that a new approach is needed to interpret contact measurements on soft materials, from characterizing cancer cells using atomic force microscopy to soft-adhesives development [32–34]. Theoretical studies have begun to investigate the contributions of surface stresses to adhesion with applied forces [10,35], but there are still only very limited experimental data [36].

In this paper, we investigate the roles of surface tension and elasticity in adhesion with applied force. We directly measure the adhesive forces and contact geometry between compliant solid substrates and small rigid spheres during quasistatic separation. We find that classic theories of contact mechanics fail to account for either the forces or the shape of the contact zone. On the other hand, the measured forces are reasonably described when a simple estimate of the contribution of surface stress is added to the standard elastic predictions. We find that the strain dependence of the solid surface stress plays an essential role in these phenomena.

We study the pull-off of small glass spheres from compliant, silicone gel substrates. The gels are prepared by mixing liquid (1 Pa s) divinyl-terminated polydimethylsiloxane (PDMS) (Gelest, DMS-V31) with a chemical cross-linker (Gelest, HMS-301) and catalyst (Gelest, SIP6831.2) (as in Refs. [11,26]). We degas the mixture in vacuum and then deposit a layer along the millimeter-wide edge of a standard microscope slide. After curing at 68 °C overnight, the resulting solid silicone substrate is about 300 μm thick, flat parallel to the long edge of the microscope slide, and very slightly curved (radius of curvature about 700 μm) in the orthogonal direction [11]. The cured PDMS substrate has a Young modulus

of $E = 5.6$ kPa, and the Poisson ratio of the gel's elastic network is $\nu = 0.48$ [11,37]. Bulk tensile tests show that the gel is linear elastic to about 10% true strain and moderately strain stiffening thereafter [38].

For rigid, spherical indenters, we use untreated silica spheres ranging in radius from 7.9 to 32.0 μm (Polysciences, 07668). We rigidly attach the spheres to the ends of either rigid, tapered glass rods or solid-state capacitive force probes (FemtoTools, FTS 100) using two-part 5-minute epoxy (Elmer's), waiting at least 6 minutes after mixing to ensure that the glue does not flow over the sphere surface. For the spheres attached to tapered glass rods, we control the position manually with submicrometer precision using a 3-axis micromanipulator stage (Narishige MMO-023). For the spheres attached to the force probes, we control the position using a 3-axis piezo stage with 1-nm accuracy (FemtoTools). Either indentation system is mounted on a standard inverted microscope, and the contact zone is imaged from the side with a 40× (N.A. 0.60) objective, as described previously [11,38].

We begin each experiment by bringing a sphere into initial adhesive contact with the solid silicone gel substrate at a vertical position $D = 0$, where D is defined as the distance between the initial, undeformed surface and the bottom of the sphere, as shown in Fig. 1(a). We approach the substrate slowly until the bottom of the sphere just touches an initially flat region of substrate that has not been contacted previously. We identify contact either as the first position where we register a measurable force on the sphere or where we visually observe the compliant substrate suddenly deforming into contact with the sphere. High-speed imaging indicates that the initial contact deformation is complete in less than a second [39]. The rigid attachment of the sphere prevents it from spontaneously indenting into the substrate [6,11], so at the start of the experiment, an initial tensile force F_0 is already required to hold the sphere at $D = 0$.

We wait about 10 minutes after initial contact in order to ensure the system is in equilibrium before beginning each experiment. We then quasistatically withdraw the sphere from the surface ($D > 0$) at a slow, controlled rate of 0.1 μm/s. A series of example images from a typical experiment on a 10.0-μm-radius sphere are shown in Fig. 1(b)–1(e). At initial contact [Fig. 1(b)], we already observe significant local deformation of the substrate. As we subsequently pull the sphere away from initial contact, the contact area stays nearly constant, decreasing only slightly as we approach the last stable position [Fig. 1(e)]. After this position, the contact line begins to slide rapidly toward a point at the bottom of the sphere where it finally
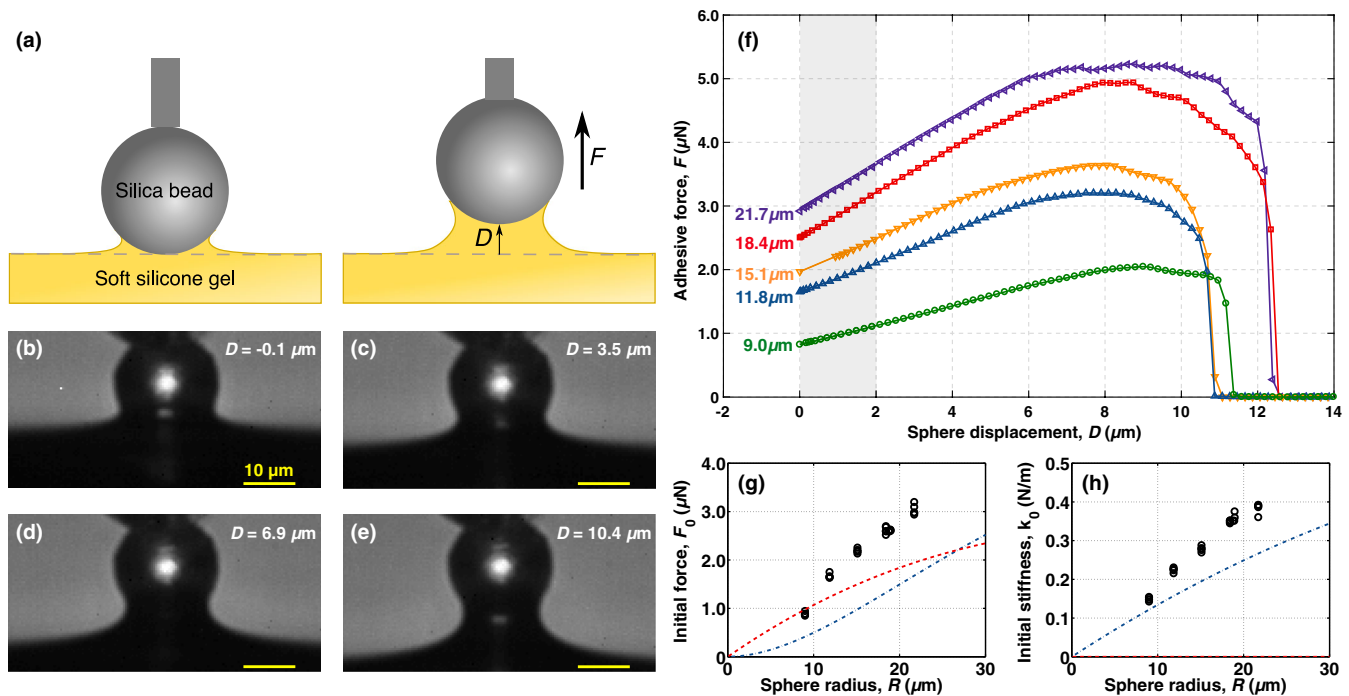
FIG. 1. Structure and force of soft adhesive contacts. (a) Schematic of the experiment. A force F is required to hold the sphere rigidly at each displacement D. (b–e) Raw images of adhesive contact between a 10.0-μm-radius sphere and an initially flat, compliant silicone substrate with a Young modulus of $E = 5.6$ kPa. (See Ref. [39] for movies of initial contact and quasistatic pull.) (f) Examples of force-displacement measurements for a range of sphere sizes from initial contact through detachment. Sphere radii are labeled. The shaded region indicates the part of the stable contact regime that is fit to measure the initial contact stiffness. (g,h) Initial contact force F_0 and initial contact stiffness k_0 plotted vs sphere radius R, respectively. Elastic contact mechanics predictions [17] are overlaid as blue dot-dashed lines. Simple capillary predictions with a fixed value of surface stress, $\Upsilon \approx 0.02$ N/m [11], are plotted as red dashed lines.

detaches. For smaller displacements, the solid adhesive bridge between the bulk of the substrate and the sphere is stable.

Examples of raw force-displacement data from initial contact ($D = 0$) through detachment for several sphere sizes are shown in Fig. 1(f). We measure the total force F required to hold the sphere rigidly at each displacement. All force-displacement measurements start with an initial tensile contact force F_0 that increases with sphere size, as shown in Fig. 1(g). From initial contact, the force then increases linearly with displacement. The initial contact stiffness, $k_0 = dF/dD|_{D=0}$, of this springlike regime also increases with sphere size, as shown in Fig. 1(h). Varying the displacement rate to be 2× slower or up to 10× faster affects the peak force and the distance to detachment but has no measurable effect on F_0 or k_0. Repeat measurements with the same sphere in different locations are extremely consistent, varying only in the detachment regime.

If the measured adhesive forces were due entirely to elastic restoring stresses, we could estimate the total force using classic adhesive contact mechanics as extended by Maugis for large contact radii [17]:

$$F_{EL} = \frac{2Ea}{1 - \nu^2} \left[-D - \frac{R}{2} + \frac{R^2 - a^2}{4a} \ln \frac{R + a}{R - a} \right]. \quad (1)$$

We use this relation to calculate elastic theory predictions for both initial contact force $F_{0,EL}(R)$ and initial contact stiffness $k_{0,EL}(R)$, overlaid on our data as blue dot-dashed lines in Figs. 1(g) and 1(h). To generate a smooth curve, we interpolate the measured contact radii (as described in Ref. [39]). Since a is only very weakly dependent on D, decreasing $\lesssim 10\%$ over the entire stable contact regime, we approximate it as constant for small D in estimating $k_{0,EL}(R)$.

Elastic theory consistently underestimates both the initial contact forces and the initial contact stiffness. One could improve the elastic calculation by accounting for nonlinear elasticity or large deformations using finite elements [35,40]. Instead, we consider possible contributions to the force from solid surface stresses.

In the absence of a complete elastocapillary adhesion theory, we calculate the capillary force contribution as the integral of the surface stresses Υ at the contact line [10]:

$$F_{CL} = 2\pi a \sin(\Theta)\Upsilon. \quad (2)$$

Here, Θ is the angle from the horizontal at which the surface leaves the contact line. As we have total wetting between the substrate and spheres [11], $\sin(\Theta) = a/R$, and Eq. (2) simplifies to $F_{CL} = 2\pi(a^2/R)\Upsilon$. Note that this is the familiar approach to determining the force exerted by a liquid bridge [41,42].

We plot the predictions of this capillary theory as red dashed lines in Figs. 1(g) and 1(h), again assuming $a \approx a_0$

for small D. For this calculation, we use the measured zero-force surface tension, $\Upsilon_0 \approx 0.02$ N/m [11]. The capillary prediction for the initial force is significant, of the same order of magnitude or larger than the elastic predictions. This additional restoring force roughly accounts for the entire discrepancy between the measured initial contact forces and the elastic predictions. However, because Eq. (2) lacks any explicit dependence on sphere displacement, this simple contact line force model does not contribute to the contact stiffness, which remains underestimated.

To gain more insight into the interplay of elastic and surface stresses during soft adhesion with applied force, we examine the structure of the contact zone. From the raw image data, we map the dark profile of the sphere and silicone substrate with 100-nm resolution using edge detection in MATLAB [11]. We also map the undeformed surface before and after the experiment to establish the zero position of the coordinate system and to check for any permanent deformation or image drift. Figure 2(a) shows the measured substrate surface profiles (overlapping gray points) extracted from the raw image examples in Figs. 1(b)–1(e), shifted so that the sphere remains in a fixed position (black circle). Since the deformation is axisymmetric, each 2D profile contains the full 3D deformation profile.

The elastic theories of contact mechanics make predictions not only for the expected forces but also for the substrate deformation profile as a function of sphere radius, contact radius, and elastic moduli [17]. We plot these predictions with no free parameters as blue lines on the left side of Fig. 2(a). For all deformations, we find that the elastic theory works well in the far field but fails to describe the shape of the surface close to the contact line. Fitting with the Maugis theory by allowing the contact radius or sphere position to vary only does a marginally better job in describing the substrate deformation.

Even though the silicone meniscus below the sphere is solid, it bears a remarkable resemblance to a liquid capillary bridge. Inspired by this similarity, we test how well a purely capillary theory describes this shape by fitting it with a surface of constant total curvature κ starting from the contact line [11]. We plot these fits as red lines on the right side of Fig. 2(a), extending the curves beyond the fit region to make it clear where they begin to deviate from the data. Note that the measured total curvatures are typically nonzero, and that they change with sphere displacement. Unlike a liquid, an elastic solid can sustain internal pressure gradients, so it does not need to have the same curvature everywhere. In control experiments with un-cross-linked PDMS fluid in the same experimental geometry, we find that the pure capillary solution works everywhere with a total curvature of zero, independent of sphere position, as expected for a liquid meniscus equilibrated with a flat far field in the absence of gravity.

The pure capillary solution fits the measured surface profile of the soft solid extremely well close to the contact
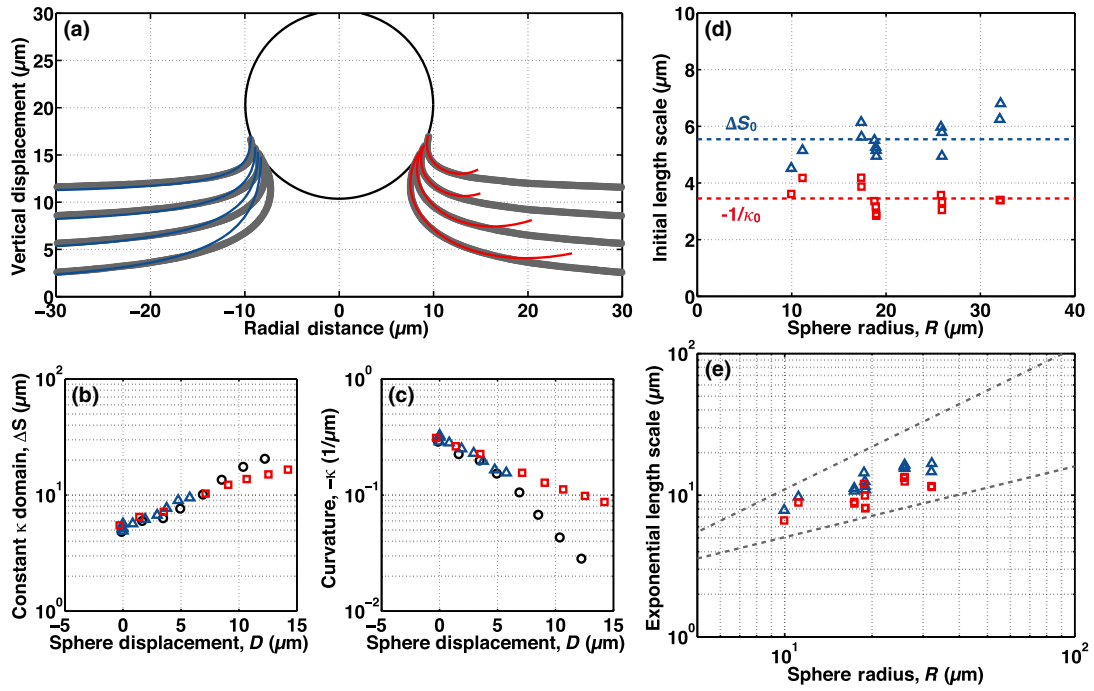
FIG. 2. Geometry of soft adhesive contact. (a) Mapped profiles from the same images shown in Figs. 1(b)–1(e) (overlapping gray points). Predictions from elastic theory [17] are overlaid on the left (blue lines). Constant total curvature fits are overlaid on the right (red lines). (b) Size of the domain of constant curvature ΔS vs sphere displacement D for three example experiments with spheres of radius 10.0 μm (black circles), 18.8 μm (blue triangles), and 32.0 μm (red squares). (c) Total curvature $-\kappa$ vs D for the same three examples as in (b). (d) Plot of fit initial length scales vs sphere radius R: ΔS_0 (blue triangles, mean $\pm$ std dev $= 5.5 \pm 0.6$ μm) and $-1/\kappa_0$ (red squares, mean $\pm$ std dev $= 3.5 \pm 0.4$ μm). (e) Log-log plot of fit exponential length scales $L_{\Delta S}$ (blue triangles) and L_κ (red squares) vs R. Lines of slope 1 (dot-dashed line) and slope 1/2 (dashed line) are shown as guides to the eye.

line, precisely where the elastic solution fails, but it deviates from the measured profile in the far field, where the elastic solution works well. We quantify the size of this domain of constant curvature, ΔS, by measuring the path length along the profile from the contact line to the end of where the capillary solution fits well. We plot ΔS and $-\kappa$ vs sphere displacement D over the entire stable contact regime in Figs. 2(b) and 2(c) for the same experiment as in Fig. 2(a) (black circles), as well as for an 18.8-μm-radius sphere (blue triangles) and a 32.0-μm-radius sphere (red squares). The domain of constant curvature expands roughly exponentially with displacement; simultaneously, the magnitude of the curvature drops roughly exponentially.

We plot the sphere-size dependence of the domain size, ΔS, and the magnitude of the curvature, $-\kappa$, at $D = 0$ in Figs. 2(d) and 2(e). Over a factor of 3 in particle radius, the initial inverse curvature (red squares) remains unchanged, while the domain of constant curvature (blue triangles) increases slightly. The initial size of the capillary-dominated domain is $\Delta S_0 = 5.5 \pm 0.6$ μm, while the initial inverse curvature at $D = 0$ is $-1/\kappa_0 = 3.5 \pm 0.4$ μm. These values are both comparable to the expected zero-force elastocapillary length: $\Upsilon_0/E = 3.6$ μm.

We plot fitted values of length scales associated with the exponential growth or decay of the domain size (blue

triangles) and curvature magnitude (red squares) on a log-log scale in Fig. 2(e). Both of these values display a roughly square-root dependence on the sphere radius over this range of sphere sizes. Consequently, an additional length scale emerges from the dependence of the contact geometry on the sphere displacement. By fitting the exponential length scales to a function of the form $L = \sqrt{lR}$, we obtain values for this new length scale of $l_{\Delta S} \approx 8.2$ μm and $l_\kappa \approx 5.2$ μm, both 1.5$\times$ larger than their corresponding initial length scales.

The contact profiles demonstrate a crossover from a capillary-dominated near field to an elastically-dominated far field, typical of elastocapillary behavior in soft materials. The transition between these domains is determined by the elastocapillary length, which is usually assumed to be a material constant [30]. Here, the dramatic increase of ΔS with sphere displacement suggests a concomitant increase in the elastocapillary length with deformation. There are two ways that the elastocapillary length can grow with strain: Either the elastic modulus drops, or the surface stress increases. Bulk tensile tests rule out the former, showing instead moderate strain stiffening at large strains. Therefore, a growing elastocapillary length can only arise from a strain-dependent surface stress that increases with substrate surface deformation.

Inspired by these observations, we recently completed a complementary study directly measuring the strain-dependent surface stress of similar silicone gels and found that it is indeed very sensitive to the surface strain of the material [38]. In that case, we found that the strain dependence is described by a surface modulus Λ such that $\Upsilon(\epsilon) = \Upsilon_0 + \epsilon\Lambda$, where $\Lambda \approx 6\Upsilon_0$. The surface modulus also introduces a new length scale Λ/E, which, for the silicone gels used in that study, is about 6 times the zero-strain elastocapillary length.

Armed with these insights into the strain dependence of the surface stress, we revisit our estimate of capillary contributions to adhesive forces. The complex strain state of these adhesion experiments makes a direct measurement of the surface modulus very difficult. We therefore estimate the scaling of Υ with D by taking the size of the domain of constant curvature as an approximate measure of the elastocapillary length. Thus, we estimate the effective surface stress for a given deformation to be simply $\Upsilon \approx \Upsilon_0 \Delta S/\Delta S_0$. Inserting this into Eq. (2) and using the mean values of the exponential fit parameters, we recalculate the capillary contributions to the total adhesive force over this range of sphere sizes, plotted as red dashed lines in Figs. 3(a) and 3(b). As implemented, the strain dependence of the surface stress has no impact on the force at initial contact [Fig. 3(a)]. However, it significantly impacts the

stiffness of the contact [Fig. 3(b)]. The sum totals of the elastic and strain-dependent capillary contributions are plotted as solid gray lines in Figs. 3(a) and 3(b). Although these are simple calculations, they capture the magnitude and scaling of both adhesive force and contact stiffness over this range of particle sizes.

This approach does remarkably well even at large deformations. We plot the measured force-displacement data for a single example experiment as black circles in Fig. 3(c). For comparison, we calculate all of the variants of the force predictions, using the contact radius and growth of the constant curvature domain as measured from the images for this experiment: the elastic prediction F_{EL} [17] (blue dot-dashed line); the capillary predictions F_{CL}, with both a fixed value of surface stress $\Upsilon = \Upsilon_0$ (red dot-dashed line) and a strain-dependent surface stress $\Upsilon \approx \Upsilon_0 \exp(D/L_{\Delta S})$ (red dashed line); and the sum total forces, using both the fixed value of surface stress (gray dot-dashed line) and the strain-dependent surface stress (gray solid line). The estimate with a fixed $\Upsilon = \Upsilon_0$ increasingly fails to describe the data as D becomes large. However, the total force combining elastic and strain-dependent capillary contributions is in remarkable agreement with the measurements again, despite the simplicity of our approach.

We have seen that theories of contact mechanics accounting only for bulk elasticity capture neither adhesive forces nor contact geometry in soft adhesion. Rather, capillary forces arising from the surface stress of the compliant solid can contribute significantly to the total force. However, simply including a fixed surface tension is not enough. Strain-dependent surface stresses are required to account for the structure and stiffness of soft adhesive contacts. While our simple estimate of contact forces does a surprisingly good job, a complete elastocapillary theory of adhesion including strain-dependent surface stress needs to be developed. In particular, contributions from the interfacial curvature through the generalized Laplace-Young relation may need to be considered [30].

FIG. 3. Predicting adhesive forces. (a,b) Initial force F_0 and initial contact stiffness k_0, respectively, vs sphere radius R. Plotted are measured data (black symbols), predictions of elastic theory (blue dot-dashed lines) [17], and capillary force predictions accounting for a strain-dependent surface stress (red dashed lines). Solid gray lines show the sum of the capillary and elastic predictions. (c) Measured force vs sphere displacement for an example experiment using an 18.9-μm-radius sphere (black points). Theoretical predictions are overlaid as follows: elastic theory (blue dot-dashed line), capillary prediction with constant or strain-dependent surface stress (red dot-dashed line and red dashed line, respectively), and total estimated force with constant or strain-dependent surface stress (gray dot-dashed line and solid gray line, respectively).

[1] C. Creton and E. Papon, *Materials Science of Adhesives: How to Bond Things Together*, MRS Bull. **28**, 419 (2003).

[2] C. Creton, *Pressure-Sensitive Adhesives: An Introductory Course*, MRS Bull. **28**, 434 (2003).

[3] S. Rose, A. Prevoteau, P. Elzière, D. Hourdet, A. Marcellan, and L. Leibler, *Nanoparticle Solutions as Adhesives for Gels and Biological Tissues*, Nature (London) **505**, 382 (2014).

[4] K. R. Shull, D. Ahn, W. L. Chen, C. M. Flanigan, and A. J. Crosby, *Axisymmetric Adhesion Tests of Soft Materials*, Macromol. Chem. Phys. **199**, 489 (1998).

[5] A. Chakrabarti and M. K. Chaudhury, *Direct Measurement of the Surface Tension of a Soft Elastic Hydrogel: Exploration of Elastocapillary Instability in Adhesion*, Langmuir **29,** 6926 (2013).

[6] R. W. Style, C. Hyland, R. Boltyanskiy, J. S. Wettlaufer, and E. R. Dufresne, *Surface Tension and Contact with Soft Elastic Solids*, Nat. Commun. **4,** 2728 (2013).

[7] T. Salez, M. Benzaquen, and É. Raphaël, *From Adhesion to Wetting of a Soft Particle*, Soft Matter **9,** 10699 (2013).

[8] X. Xu, A. Jagota, and C.-Y. Hui, *Effects of Surface Tension on the Adhesive Contact of a Rigid Sphere to a Compliant Substrate*, Soft Matter **10,** 4625 (2014).

[9] Z. Cao, M. J. Stevens, and A. V. Dobrynin, *Adhesion and Wetting of Nanoparticles on Soft Surfaces*, Macromolecules **47,** 3203 (2014).

[10] C.-Y. Hui, T. Liu, T. Salez, E. Raphael, and A. Jagota, *Indentation of a Rigid Sphere into an Elastic Substrate with Surface Tension and Adhesion*, Proc. R. Soc. A **471,** 20140727 (2015).

[11] K. E. Jensen, R. Sarfati, R. W. Style, R. Boltyanskiy, A. Chakrabarti, M. K. Chaudhury, and E. R. Dufresne, *Wetting and Phase Separation in Soft Adhesion*, Proc. Natl. Acad. Sci. U.S.A. **112,** 14490 (2015).

[12] T. Liu, A. Jagota, and C.-Y. Hui, *Adhesive Contact of a Rigid Circular Cylinder to a Soft Elastic Substrate—The Role of Surface Tension*, Soft Matter **11,** 3844 (2015).

[13] P. C. Nalam, N. N. Gosvami, M. A. Caporizzo, R. J. Composto, and R. W. Carpick, *Nano-Rheology of Hydrogels Using Direct Drive Force Modulation Atomic Force Microscopy*, Soft Matter **11,** 8165 (2015).

[14] H. K. Minsky and K. T. Turner, *Composite Microposts with High Dry Adhesion Strength*, ACS Appl. Mater. Interfaces **9,** 18322 (2017).

[15] K. L. Johnson, K. Kendall, and A. D. Roberts, *Surface Energy and Contact of Elastic Solids*, Proc. R. Soc. A **324,** 301 (1971).

[16] K. L. Johnson and K. K. L. Johnson, *Contact Mechanics* (Cambridge University Press, Cambridge, England, 1987).

[17] D. Maugis, *Extension of the Johnson-Kendall-Roberts Theory of the Elastic Contact of Spheres to Large Contact Radii*, Langmuir **11,** 679 (1995).

[18] D. Long, A. Ajdari, and L. Leibler, *Static and Dynamic Wetting Properties of Thin Rubber Films*, Langmuir **12,** 5221 (1996).

[19] S. Mora, T. Phou, J.-M. Fromental, L. M. Pismen, and Y. Pomeau, *Capillarity Driven Instability of a Soft Solid*, Phys. Rev. Lett. **105,** 214301 (2010).

[20] E. R. Jerison, Y. Xu, L. A. Wilen, and E. R. Dufresne, *Deformation of an Elastic Substrate by a Three-Phase Contact Line*, Phys. Rev. Lett. **106,** 186103 (2011).

[21] A. Jagota, D. Paretkar, and A. Ghatak, *Surface-Tension-Induced Flattening of a Nearly Plane Elastic Solid*, Phys. Rev. E **85,** 051602 (2012).

[22] R. W. Style, R. Boltyanskiy, Y. Che, J. S. Wettlaufer, L. A. Wilen, and E. R. Dufresne, *Universal Deformation of Soft Substrates near a Contact Line and the Direct Measurement of Solid Surface Stresses*, Phys. Rev. Lett. **110,** 066103 (2013).

[23] N. Nadermann, C.-Y. Hui, and A. Jagota, *Solid Surface Tension Measured by a Liquid Drop under a Solid Film*, Proc. Natl. Acad. Sci. U.S.A. **110,** 10541 (2013).

[24] D. Paretkar, X. Xu, C.-Y. Hui, and A. Jagota, *Flattening of a Patterned Compliant Solid by Surface Stress*, Soft Matter **10,** 4084 (2014).

[25] Z. Cao, M. J. Stevens, and A. V. Dobrynin, *Elastocapillarity: Adhesion and Wetting in Soft Polymeric Systems*, Macromolecules **47,** 6515 (2014).

[26] R. W. Style, R. Boltyanskiy, B. Allen, K. E. Jensen, H. P. Foote, J. S. Wettlaufer, and E. R. Dufresne, *Stiffening Solids with Liquid Inclusions*, Nat. Phys. **11,** 82 (2015).

[27] B. Andreotti and J. H. Snoeijer, *Soft Wetting and the Shuttleworth Effect, at the Crossroads between Thermodynamics and Mechanics*, Europhys. Lett. **113,** 66001 (2016).

[28] Z. Cao and A. V. Dobrynin, *Nanoparticles as Adhesives for Soft Polymeric Materials*, Macromolecules **49,** 3586 (2016).

[29] J. Long, G. Wang, X.-Q. Feng, and S. Yu, *Effects of Surface Tension on the Adhesive Contact between a Hard Sphere and a Soft Substrate*, Int. J. Solids Struct. **84,** 133 (2016).

[30] R. W. Style, A. Jagota, C.-Y. Hui, and E. R. Dufresne, *Elastocapillarity: Surface Tension and the Mechanics of Soft Solids*, Annu. Rev. Condens. Matter Phys. **8,** 99 (2017).

[31] M. Ina, Z. Cao, M. Vatankhah-Varnoosfaderani, M. H. Everhart, W. F. M. Daniel, A. V. Dobrynin, and S. S. Sheiko, *From Adhesion to Wetting: Contact Mechanics at the Surfaces of Super-Soft Brush-like Elastomers*, ACS Macro Lett. **6,** 854 (2017).

[32] K. J. Van Vliet, G. Bao, and S. Suresh, *The Biomechanics Toolbox: Experimental Approaches for Living Cells and Biomolecules*, Acta Mater. **51,** 5881 (2003).

[33] K. R. Shull, *Contact Mechanics and the Adhesion of Soft Solids*, Mater. Sci. Eng., R **36,** 1 (2002).

[34] D. M. Ebenstein and K. J. Wahl, *A Comparison of JKR-Based Methods to Analyze Quasi-static and Dynamic Indentation Force Curves*, J. Colloid Interface Sci. **298,** 652 (2006).

[35] T. Liu, A. Jagota, and C.-Y. Hui, *Effect of Surface Tension on the Adhesion between a Rigid Flat Punch and a Semi-infinite Neo-hookean Half-Space*, Extreme Mech. Lett. **9,** 310 (2016).

[36] J. T. Pham, F. Schellenberger, M. Kappl, and H.-J. Butt, *From Elasticity to Capillarity in Soft Materials Indentation*, Phys. Rev. Mater. **1,** 015602 (2017).

[37] R. W. Style, R. Boltyanskiy, G. K. German, C. Hyland, C. W. MacMinn, A. F. Mertz, L. A. Wilen, Y. Xu, and E. R. Dufresne, *Traction Force Microscopy in Physics and Biology*, Soft Matter **10,** 4047 (2014).

[38] Q. Xu, K. E. Jensen, R. Boltyanskiy, R. Sarfati, R. W. Style, and E. R. Dufresne, *Direct Measurement of Strain-Dependent Solid Surface Stress*, Nat. Commun. **8,** 555 (2017).

[39] See Supplemental Material at http://link.aps.org/supplemental/10.1103/PhysRevX.7.041031 for movies of initial contact and quasistatic pull, as well as measurements of contact radii vs sphere radii and vs sphere displacement.

[40] X. Xu, *Effect of Surface Tension on Deformation of Soft Solids* (Cornell University, Ithaca, 2016).

[41] P.-G. De Gennes, F. Brochard-Wyart, and D. Quéré, *Capillarity and Wetting Phenomena: Drops, Bubbles, Pearls, Waves* (Springer Science & Business Media, New York, 2013).

[42] H.-J. Butt and M. Kappl, *Surface and Interfacial Forces* (John Wiley & Sons, New York, 2009).